JOURNAL OF THERMOPHYSICS AND HEAT TRANSFER
Vol. 9, No. 1, January–March 1995

Characterization of Arcjet Flows Using Laser-Induced Fluorescence

Douglas J. Bamford*
Deacon Research, Palo Alto, California 94303
Anthony O'Keefe†
Los Gatos Research, Los Gatos, California 95030
and
Dikran S. Babikian,‡ David A. Stewart,§ and Anthony W. Strawa¶
NASA Ames Research Center, Moffett Field, California 94035

A sensor based on laser-induced fluorescence has been installed at the 20-MW NASA Ames Aerodynamic Heating Facility. The sensor has provided new, quantitative, real-time information about properties of the arcjet flow in the highly dissociated, partially ionized, nonequilibrium regime. Number densities of atomic oxygen, flow velocities, heavy particle translational temperatures, and collisional quenching rates have been measured. These results have been used to test and refine computational models of the arcjet flow. The calculated number densities, translational temperatures, and flow velocities are in moderately good agreement with experiment.

Nomenclature

A = Einstein A coefficient in Eqs. (2) and (3)
A_H = constant used to calculate $\langle d\sigma/d\Omega \rangle$ in Eq. (9)
c = speed of light
D = Raman calibration constant defined by Eq. (7)
dm/dt = arc heater mass flow rate
$\langle d\sigma/d\Omega \rangle$ = Raman scattering cross section for H_2
E = energy per laser pulse in laser-induced fluorescence experiment
$E_{J''}$ = energy of the fine structure level with quantum number J''
E_0 = energy per laser pulse in Raman calibration
$F(t)$ = relative laser intensity as a function of time, normalized according to Eq. (5)
G_a/C = preamplifier gain/capacitance ratio
G_p = photomultiplier tube gain
$G^{(2)}$ = second-order autocorrelation function of laser field
$g_{J''}$ = degeneracy of lower-state fine structure level
H_T = mass-averaged enthalpy
$h\nu$ = energy per uv laser photon in laser-induced fluorescence experiment
$h\nu_s$ = energy of Raman-scattered photon
I = arc heater current
$I_{J''}$ = integrated LIF intensity for the $3p^3P_{2,1,0} \leftarrow 2p^3P_{J''}$ transition
J' = angular momentum quantum number in excited electronic state
J'' = angular momentum quantum number in lower electronic state
k_e = rate constant for quenching by electrons
k_q = rate constant for quenching by neutral species
L = length of region over which fluorescence is observed
M_f = frozen Mach number
N_e = number density of electrons
N_H = number density of H_2
N_N = number density of atomic nitrogen
N_{tot} = number density of neutral species
N_0 = number density of atomic oxygen
q = electron charge
S = preamplifier signal voltage
t = time during laser pulse in Eq. (5)
V = arc heater voltage
v = flow velocity
$\Delta\lambda_\theta$ = splitting between O-atom absorption line and NO absorption line at a particular value of θ
$\Delta\lambda_{90}$ = splitting between O-atom absorption line and NO absorption line at $\theta = 90$ deg
η = arc heater efficiency
η_t = transmission of windows and filters
η_ϕ = photomultiplier tube quantum efficiency
θ = angle between laser propagation direction and flow direction
λ = laser wavelength
ν_i = constant used to calculate $\langle d\sigma/d\Omega \rangle$ in Eq. (9)
ν_p = wave number for pump photon
ν_s = wave number for Stokes photon
$\sum \sigma_0^{(2)}$ = integrated two-photon absorption cross section for the $3p^3P_{2,1,0} \leftarrow 2p^3P_2$ transition
$\hat{\sigma}^{(2)}$ = two-photon absorption cross section
ϕ_f = fluorescence quantum yield
Ω_0 = solid angle of fluorescence collection system
ω = two-photon frequency, $4\pi c/\lambda$
ω_h = laser beam spot size in horizontal direction
ω_v = laser beam spot size in vertical direction

Presented as Paper 94-0690 at the AIAA 32nd Aerospace Sciences Meeting, Reno, NV, Jan. 10–13, 1994; received April 26, 1994; revision received July 11, 1994; accepted for publication July 18, 1994.
Copyright © 1994 by the American Institute of Aeronautics and Astronautics, Inc. All rights reserved.
*Research Physicist, Thermosciences Division. Member AIAA.
†President. Member AIAA.
‡Research Scientist, Thermosciences Institute. Member AIAA.
§Research Scientist, Earth System Science Division. Member AIAA.
¶Research Scientist, Earth System Science Division. Senior Member AIAA.

Introduction

ARCJETS have been used for many years to simulate the re-entry environment in the laboratory.[1] The arc flow

conditions are tailored to simulate the conditions to be encountered by the model material during re-entry, and the response of the material to these conditions is studied. The material must be able to withstand the heating caused by radiation, convection, and surface recombination of the species contained in the shock. All of the existing thermal protection materials, such as the Space Shuttle tiles, were developed using this type of testing. The aerothermodynamic states of the flows in arcjet facilities are not known well enough to allow realistic simulations of future space missions that will encounter more severe heating and more serious departures from chemical equilibrium.[2]

The experiments described here are designed to add to the existing body of knowledge of arcjet properties,[3] which in turn will be used to test and refine computational models of the arcjet flow. Before this work, number densities of major species had never been measured in the freestream of any arcjet flow; two of these species, O($2p^3P$) and N($2p^4S^0$), had never been directly observed. Translational temperatures and flow velocities of atomic copper were measured previously at the Johnson Space Center (JSC).[4,5] Because the copper velocities were lower than predictions, and because the flow conditions at NASA Ames are substantially different from those at JSC, further measurements and calculations must be carried out before the flow velocities can be understood. After atomic copper was found to be an unreliable probe in the Ames arc heater (A. O'Keefe and D. J. Bamford, unpublished results), atomic oxygen was used as the target species for velocity and temperature measurements.

Experiment

The 20-MW NASA Ames Aerodynamic Heating Facility has been described in detail elsewhere.[6] A constricted arc heater and a conical nozzle are used to provide dissociated hypersonic flow over test models in the test section of the facility. Freestream conditions in the test section are varied by changing the size of the throat, the size of the nozzle exit, the reservoir pressure, or the electrical power dissipated in the arc heater. The nozzle geometric area ratio (exit-to-throat) can be varied from 64 to 400, whereas the reservoir pressure can be varied from 1.0 to 5.5 atms. The maximum power dissipation is 20 MW. The facility uses either air or nitrogen, mixed with argon, as the test gas.

The experiments are aimed at detecting two of the most important constituents of the flow: 1) atomic oxygen and 2) atomic nitrogen, using laser-induced fluorescence (LIF). The basic approach can be explained with reference to the energy level diagrams for atomic oxygen and nitrogen in Fig. 1. Oxygen atoms in the ground electronic state are excited via the $3p^3P_{2,1,0} \leftarrow 2p^3P_2$ two-photon transition at 225.7 nm, and detected using the $3p^3P_{2,1,0} \rightarrow 3s^3S_1^0$ fluorescence transition at 844.5 nm. Nitrogen atoms are excited using the $3p^4D^0 \leftarrow 2p^4S^0$ two-photon transition at 211 nm and detected via the $3p^4D^0 \rightarrow 3s^4P$ transition at 869 nm.

A schematic diagram of the LIF sensor is shown in Fig. 2. A frequency-tripled Nd:YAG laser (Continuum NY81) pumps a tunable dye laser (Continuum ND60, Dual Grating Option). For oxygen atom detection the dye laser (Coumarin 460 laser dye) produces tunable radiation in the 452-nm region. When nitrogen atoms are detected, Stilbene 420 dye is used to produce tunable radiation near 422 nm. The tunable blue radiation is frequency-doubled in a crystal of beta-barium borate (BBO) to produce the appropriate uv wavelength. The uv radiation is separated from residual blue radiation with a Pellin-Broca prism, and then reflected off three dielectric mirrors (only one of which is shown in the figure), toward the large vacuum chamber that comprises the test cell. The laser beam is shaped by a telescope consisting of two fused silica lenses to form a nearly collimated beam of the appropriate diameter. It then passes through an assembly containing an optically flat fused silica window and down into the test cell. The laser is linearly polarized, with its electric field vector usually lying parallel to the flow direction. The angle between the laser direction and the flow direction can be varied by moving the window assembly from one flange to another on top of the test cell. A small amount of uv radiation transmitted by the first dielectric mirror is directed onto a pyroelectric energy meter (Molectron J3-09) to measure pulse-to-pulse fluctuations in the laser energy.

Laser-induced fluorescence is detected at right angles to the laser and flow directions. The fluorescence passes through a glass window on the west side of the test cell. A fused silica lens (f = 35 cm) located about 200 cm from the observation point is used to image the fluorescence onto the surface of a red-sensitive photomultiplier tube (Hamamatsu R636). A circular aperture of variable size in front of the photomultiplier tube (PMT) serves to define the observation region. This region is located 25 cm downstream from the nozzle exit, and 10 cm upstream of the test model position. An optical interference filter (Corion S10-850-S for O-atoms, Corion S10-870-S for N-atoms) transmits light at the wavelength of interest and blocks light at other wavelengths.

A separate beam path is used to determine the dye laser wavelength. A small amount of uv radiation reflected from the incident face of the Pellin-Broca prism is separated from residual blue light by a 90-deg prism. The uv radiation is then directed into a small stainless cell filled with nitric oxide. Laser-induced fluorescence from the nitric oxide is detected by a photomultiplier tube (Hamamatsu R928). An uv-transmitting filter (Schott UG11) is used to prevent scattered laser

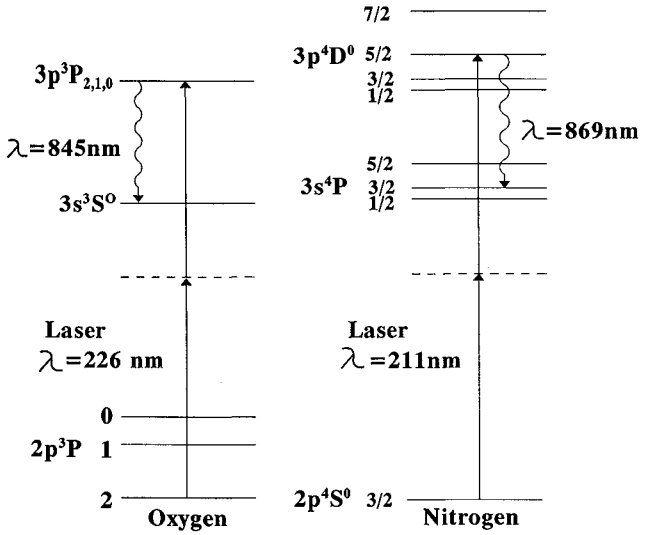

Fig. 1 Energy level diagrams for atomic oxygen and nitrogen.

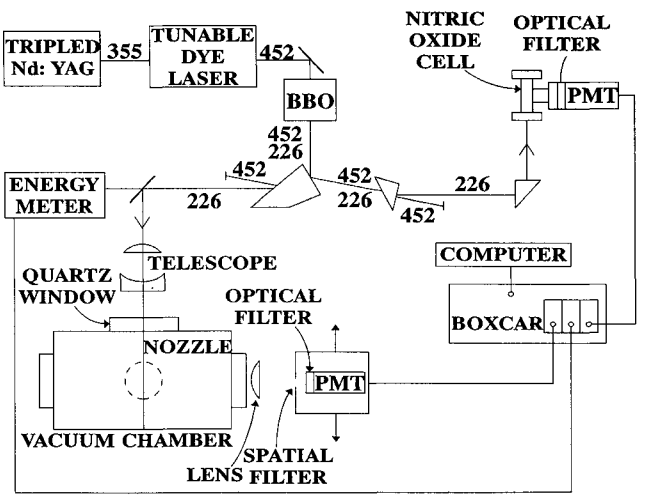

Fig. 2 Schematic diagram (not drawn to scale) of the flow sensor.

light from reaching the PMT. The absolute wavelengths are determined from the nitric oxide molecular constants and line positions given by Engleman et al.[7]

Signals are processed using a Stanford Research Systems data acquisition system. Three gated integrators (SR250), located in an SR280 boxcar mainframe, receive signals from three detectors (arcjet PMT, nitric oxide PMT, and pyroelectric energy meter). In some cases the signals pass through a preamplifier (Ortec 113, Ortec 9305, or SRS SR240) prior to the gated integrator. Output voltages from the gated integrators are digitized and transferred to a microcomputer via an SR245 computer interface.

The interpretation of the two-photon LIF results draws upon procedures developed earlier to measure two-photon absorption cross sections.[8,9] A pulse from the narrow-band laser source excites the atoms at the peak of the Doppler absorption profile, and the fluorescence resulting from that pulse is detected by a photomultiplier tube. The fraction of atoms excited during the pulse depends on the spatial and temporal characteristics of the laser source and on the Doppler width.[9-11] The fraction of excited atoms that fluoresce at this wavelength (the fluorescence quantum yield ϕ_f) will depend on the rates of competing processes including collisional quenching, stimulated emission, and absorption of a third photon into the ionization continuum. The laser intensity is maintained at relatively low value, at which neither the two-photon transition nor the subsequent transition to the ionization continuum is saturated, and at which stimulated emission (also called "amplified spontaneous emission" or ASE) is insignificant. Rate equations are used to describe the interaction of the atoms with the radiation field, as was done previously,[9] to measure absolute number densities. To measure O-atom fine structure temperature, the relative intensities of transitions originating from the three fine structure levels in the ground electronic state are measured. To determine velocities, the Doppler shift of the O-atom resonance at a fixed angle between the laser direction and the flow direction is measured.

Theory

Two different computer codes have been used to interpret the experimental results. The first code provides an approximate solution that ignores detailed chemical processes in the expanding flow. Because it allows rapid calculations to be made, the code is used to develop an intuitive understanding of the effect of changing arc heater conditions on the flow properties. The second code accounts for detailed chemical processes and provides more accurate results.

The first code combines a one-dimensional flow code developed by Yoshikawa and Katzen,[12] Gupta's thermodynamic properties,[13] and the Aerotherm Chemical Equilibrium (ACE) program.[14] This code uses M_f to define the state of the gas and its properties relative to location in the conical nozzle or test section of the facility. Most properties of the gas, having undergone relaxation of several internal degrees of freedom (DOF), are assumed to be approximately the same as if the gas had made an instantaneous transition from full equilibrium flow to flow in which all internal energy exchanges are frozen. The frozen Mach number specifies the equilibrium speed of sound and the constant entropy at which the expanding gas has made its transition to an internally frozen flow. Higher values of M_f correspond to flows closer to equilibrium chemistry. The calculations assume $M_f = 1.0$, corresponding to freezing at the nozzle entrance.

The second code, entitled NOZNT,[15] solves a one-dimensional steady flow through a convergent-divergent nozzle in the dissociated and ionized regime. It assumes the entrance and the beginning section of the nozzle to be at equilibrium. The rest of the flow is solved assuming multitemperature nonequilibrium flow. The equilibrium portion of the flow is solved with the pressure-specified method. Nonequilibrium calculations of the flow are started in the converging portion of the nozzle upstream of the throat. The nonequilibrium calculation also uses the pressure-specified method up to the point where $M_f = 1.8$. From this point the area-specified method is used. In this region of the flow the equations for conservation of species, vibrational energy, and electron-electronic energy are solved numerically.

Different methods for calculating the enthalpy are used in the two computer codes. In the ACE calculations, the enthalpy distribution across the hypersonic stream in the test section is assumed to vary directly with the heating rate measured at the stagnation point of a 2.54-cm-diam hemisphere. The mass-averaged and centerline enthalpies are then calculated using energy balance and mass flow relationships for the arc heater. In this method, the centerline enthalpies are about 15% higher than the mass-averaged enthalpies. The mass-averaged enthalpy is calculated according to the following equation:

$$H_T = \eta VI \left(\frac{dm}{dt}\right) \tag{1}$$

Values of η, as a function of flow conditions, are interpolated from cooling water temperature-rise measurements for an identical arc heater at Ames Research Center.

A different procedure is used to calculate enthalpies for the NOZNT calculations. A radial distribution of enthalpies inside the arc constrictor is calculated using the flowfield code ARCFLO.[15] The centerline enthalpy at the nozzle entrance is assumed to be half as large as the centerline enthalpy at the arc heater exit because of the mixing process in the settling chamber between the constrictor and the nozzle. This assumption was used in earlier work to obtain good agreement between observed and predicted stagnation-point heating rates and nitric oxide emission spectra.[15] In this approximation the centerline enthalpy at the nozzle entrance is larger than the calculated mass-averaged enthalpy by a factor that varies between 1.5–2.5, depending on the run conditions.

Experimental and Theoretical Results

The experiments were carried out under a variety of test conditions during twenty-three runs, which are numbered for future reference and summarized in Table 1. The throat diameter was 3.81 cm in each test. For runs 4–7, the centerline enthalpies calculated by the two methods discussed above are shown in Table 1.

Table 1 Summary of arcjet conditions

Run	I, A	P, psi	V	Nozzle diameter, cm	Centerline enthalpy, MJ/kg	
					ACE	NOZNT
1	1150	30	2700	30.5	—	—
2	2000	64	3700	61.0	—	—
3	2000	65	3700	61.0	—	—
4	1600	40	2950	61.0	22.9	30.6
5	1600	40	2900	61.0	21.2	30.3
6	2000	65	2800	61.0	15.0	31.0
7	750	20	2350	61.0	15.6	28.2
8	600	20	2600	61.0	—	—
9	800	20	2300	61.0	—	—
10	650	20	2450	61.0	—	—
11	600	20	2600	61.0	—	—
12	750	20	2500	61.0	—	—
13	725	20	2400	61.0	—	—
14	850	20	2100	61.0	—	—
15	725	20	2400	61.0	—	—
16	800	20	2250	61.0	—	—
17	1200	24	2400	30.5	—	—
18	1200	25	2500	30.5	—	—
19	1200	25	2450	30.5	—	—
20–23	1200	25	2525	30.5	—	—

Establishing Validity of Experimental Techniques

Examples of O-atom LIF signals from the $3p^3P_{J'} \leftarrow 2p^3P_{J''}$ transitions are shown in Fig. 3. The peak signal intensity decreases as J'' decreases because fine structure levels of higher energy have lower population, a trend that can be quantified using the known relative intensities[10,16] of the state-to-state fine structure transitions.

Figure 4 shows an LIF spectrum for the $3p^4D^0_{5/2} \leftarrow 2p^4S^0_{3/2}$ transition of atomic nitrogen. The solid line represents N-atom LIF, whereas the dotted line represents nitric oxide LIF. The NO lines have all been assigned to the (2,0) band of the $B^2\Pi \leftarrow X^2\Pi$ transition using constants of Engleman et al.[7]

Because the measurements of arcjet properties are not instantaneous, the degree to which atomic densities remain constant during a test had to be measured. To test for fluctuations the laser was tuned onto the peak of the $3p^3P_{2,1,0} \leftarrow 2p^3P_2$ transition, and the LIF intensity (properly normalized for energy variations) was monitored as a function of time during run 13. The data were acquired in a series of bins with 5 laser pulses averaged together per bin. The LIF intensity varied by $\pm 10\%$ about its mean value, but showed no systematic drift during the run. During run 4 the integrated intensity of the LIF spectrum was constant to within 3% in two scans taken at 4-min intervals.

Fluorescence quenching must be accounted for when relating absolute signal sizes to absolute excited state number densities. If an ensemble of excited atoms is created by a short laser pulse, the excited state number density will then decay exponentially. The exponential decay is caused by three first-order rate processes that remove population from the excited state: 1) radiative decay, 2) collisional deactivation by neutral species, and 3) collisional deactivation by electrons. The time scale on which excited atoms flow out of the observation region (several microseconds) is too long to affect the measurement. Because the fluorescence intensity is proportional to the excited state number density, it will decay exponentially with the same time constant. The exponential decay time of the fluorescence τ_f is given by the following equation:

$$\tau_f = (A + k_q N_{\text{tot}} + k_e N_e)^{-1} \tag{2}$$

A related quantity is ϕ_f, the fraction of excited atoms that decay radiatively, which is given by the following equation:

$$\phi_f = A\tau_f \tag{3}$$

The values of the Einstein A coefficients for atomic oxygen and nitrogen are well-established in the literature.[17,18] If the fluorescence lifetime τ_f is longer than the laser pulse length, then its value (and thus the value of ϕ_f) can be determined experimentally. This was the case for atomic oxygen under the entire range of test conditions used in these experiments. For atomic nitrogen the range of conditions tested was more limited and the signal-to-noise ratio was poorer, but the measured τ_f values were similar to those for atomic oxygen. Decay curves were obtained by scanning the gate on the SR250 gated integrator. For atomic oxygen, the fluorescence lifetimes ranged from 23.1 to 33.4 ns, corresponding to fluorescence quantum yields between 0.65–0.94. Atomic nitrogen fluorescence lifetimes ranged from 23.5 to 33.4 ns, corresponding to fluorescence quantum yields between 0.54–0.68. For both species the observed fluorescence lifetimes are consistent with quenching by heavy particles alone, as estimated from earlier measurements of fluorescence quenching in discharge/flow systems.[9,19]

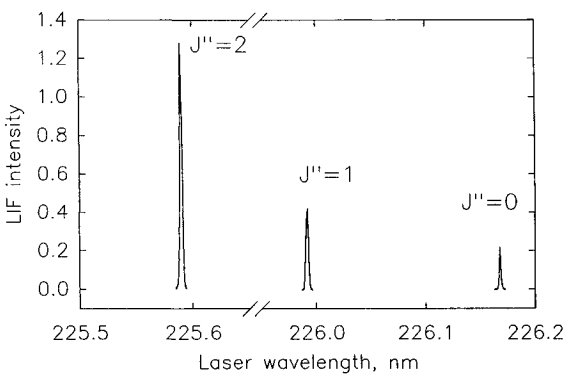

Fig. 3 Spectrum showing the $3p^3P_{2,1,0} \leftarrow 2p^3P_{J''}$ transitions in atomic oxygen, run 22.

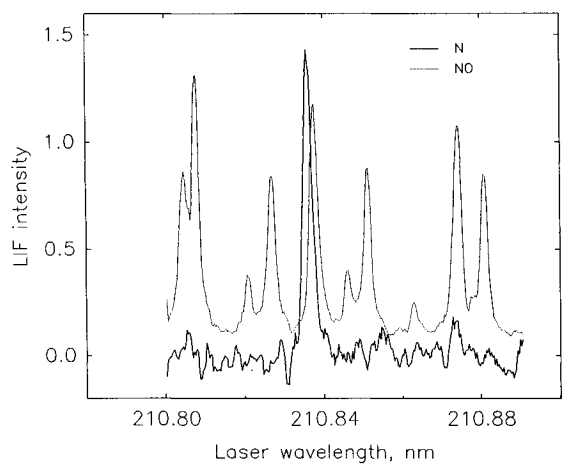

Fig. 4 LIF spectrum showing the $3p^4D^0_{5/2} \leftarrow 2p^4S^0_{3/2}$ transition in atomic nitrogen, along with a nitric oxide reference spectrum, run 17.

In any nonlinear optics experiment one must check for the presence of other optical processes that compete with the process being measured. If no other processes remove population from the excited state during the laser pulse, then the number of detected photons in a two-photon excited fluorescence experiment is proportional to the square of the laser pulse energy [Ref. 9, Eq. (28)]. Thus, a plot of the logarithm of the LIF intensity as a function of the logarithm of the laser pulse energy should yield a straight line with a slope of 2.0. The range of laser intensities over which the slope does equal 2.0 is called the "low intensity regime." On the other hand, if significant population is removed from the excited state by other optical processes such as photoionization or ASE,[20–22] then the LIF intensity at high laser pulse energies will be lower than it would be in the absence of these competing processes. The log-log plot will thus be nonlinear, with a slope that decreases as the pulse energy increases. To check for these competing processes, the laser pulse energy was varied by detuning the BBO doubling crystal while leaving everything else unchanged. A pyroelectric detector array verified that the spatial profile and position of the laser beam inside the test cell were not changed significantly by this procedure. The log-log plot of O-atom LIF signal vs laser energy was linear with a least-squares slope of 2.0, as expected in the low-intensity regime. At the highest laser energy used in this test, the peak laser intensity was comparable to the intensity used in the number density measurements, approximately 20 MW/cm^2.

Atomic Oxygen Number Density Measurement

To convert the measured O-atom LIF intensities into absolute number densities, several calibration steps were carried out. The basic approach was outlined in an earlier paper[9] on the measurement of the two-photon absorption cross section in atomic oxygen. Using a source that produced O-atoms of a known number density, the two-photon cross section was determined by carefully measuring the laser intensity and the sensitivity of the fluorescence collection system. The measured cross section agreed well with theory.[9,10] In the present experiment this sequence of steps was reversed: the known cross section was used to determine the unknown number density in the arcjet.

In earlier work[8,9] all of the equations needed to interpret the data were derived. A rearrangement of Eq. (29) of Ref. 9 leads to the following expression for the atomic oxygen number density:

$$N_0 = \left[4\pi^2 (S/E^2) \omega_v \omega_h (h\nu)^2 / \hat{\sigma}^{(2)} \phi_f D \int_{-\infty}^{\infty} F^2(t'')\, dt'' \right] \quad (4)$$

In the following paragraphs, the procedures used to measure the quantities in Eq. (4) are described.

The laser spatial profile was measured at the appropriate position inside the test cell with a Spiricon pyroelectric detector array. This device has a series of detectors spaced at 100-μm intervals. Each detector produces a voltage proportional to the local laser intensity. A reflection from a glass plate oriented near Brewster's angle was used to produce a reflection of the uv beam that was weak enough to avoid saturating the detectors. Using the array's built-in electronics, a sequence of voltages, corresponding to a sequence of intensity readings from the various detectors, was sent to the Tektronix 2467 oscilloscope. The oscilloscope readout was photographed and saved for further analysis. Rotation of the one-dimensional detector array by 90 deg allowed profiles to be obtained in the vertical and horizontal directions, where "vertical" means parallel to the flow direction.

Spatial profile data were analyzed assuming a Gaussian form for the spatial distribution, as was done previously.[9] The width of the Gaussian in the ith direction is characterized by a spot size ω_i, which is the distance from centerline at which the intensity has fallen to $(1/e^2)$ of its centerline value.

The relative laser energy was recorded during each experiment using a reading from a Molectron pyroelectric detector, as shown schematically in Fig. 2. This arrangement was adopted because an energy meter could not be placed inside the test cell during the arcjet runs. These relative readings were placed on an absolute scale after the number density experiment by comparing the boxcar-averaged Molectron readings with readings from a Scientech Astral power meter inside the test cell.

The laser temporal profile was measured using a fast photodiode (EG&G FND-100Q, biased at 90 V) along with a fast oscilloscope (Tektronix 2467). The energy of the uv beam was reduced by three near-Brewster angle reflections to avoid saturating the photodiode. As was explained previously,[9] $F(t)$ is properly normalized according to the following equation:

$$\int_{-\infty}^{\infty} F(t')\, dt' = 1 \quad (5)$$

The integral of the square of $F(t)$ was calculated from a Gaussian fit to the observed temporal profile.

To relate the observed signal strength to the number of ground-state atoms, $\hat{\sigma}^{(2)}$ must be known. This quantity depends on the degree to which the laser contains intensity fluctuations on a timescale too short to be detected. Because the two-photon excitation rate depends on the square of the instantaneous laser intensity, a laser pulse with severe intensity fluctuations will produce more excited atoms than a smooth pulse, all other factors (including pulse energy and apparent pulse length) being equal. The amount of two-photon excitation is proportional to a parameter $G^{(2)}$, which is unity for a smooth pulse and greater than 1 for a "spiky" pulse. In earlier work,[11] different 226-nm laser systems produced different values of $G^{(2)}$. Because the laser system used in the present work was not used in the earlier work, reasonable assumptions about the physics which produces "spikiness" in the various laser systems were used to conclude that $G^{(2)} = 2.2 \pm 0.8$ for the laser system used in the present experiments. The value of $G^{(2)}$ cannot be determined more precisely without carrying out measurements on an O-atom source of known density, as was done in Refs. 9 and 11.

In estimating $\hat{\sigma}^{(2)}$, the observed linewidth of the two-photon transition must be accounted for. The value of $\hat{\sigma}^{(2)}$ depends on the absolute frequency ω, depending on the spacing between ω and the atomic resonance. The normalized LIF intensity at any value of ω is proportional to $\hat{\sigma}^{(2)}$. When the transition width increases (because of Doppler broadening and/or a broader laser linewidth), the value of $\hat{\sigma}^{(2)}$ on linecenter decreases. In previous work[9] the function $\hat{\sigma}^{(2)}(\omega)$ was integrated over ω to yield the following equation:

$$\int_{-\infty}^{\infty} \hat{\sigma}^{(2)}(\omega)\, d\omega = G^{(2)} \sum \sigma_0^{(2)}(J' \leftarrow 2) \quad (6)$$

The value of the integrated two-photon absorption cross section, $(1.87 \pm 0.60) \times 10^{-35}$ cm^4, was determined in earlier work with a transform-limited laser.[10] Figure 3 was used to estimate $\hat{\sigma}^{(2)}$ on linecenter as follows. Appropriate scale factors were used to convert the graph to a plot of $\hat{\sigma}^{(2)}$ as a function of ω. The parameter $G^{(2)}$ was assumed equal to 2.2, and the peak value of $\hat{\sigma}^{(2)}$ was adjusted to make the integrated area of the transition satisfy Eq. (6).

The absolute sensitivity of the fluorescence collection system was measured by Raman scattering in hydrogen.[8] The O-atom fluorescence signal is proportional to a calibration constant D, given by the following equation:

$$D = L\Omega_0 \eta_t \eta_\phi q G_p (G_a/C) \quad (7)$$

The calibration constant is determined by filling the observation region with hydrogen, exciting the gas with a laser in the 625-nm wavelength region, and observing the first Stokes radiation in the 845-nm region.[8] This constant is given by the following equation:

$$D = \left(\frac{Sh\nu_s}{E_0 N_H \left\langle \frac{d\sigma}{d\Omega} \right\rangle} \right) \quad (8)$$

For the excitation geometry used in the Raman calibration, the scattering cross section is given by the following equation:

$$\left\langle \frac{d\sigma}{d\Omega} \right\rangle = \frac{A_H \nu_s^4}{(\nu_i^2 - \nu_p^2)^2} \quad (9)$$

where $A_H = 8.74 \times 10^{-28}$ cm^2/sr, $\nu_i = 84{,}800$ cm^{-1}, and $\nu_s = \nu_p - 4155$ cm^{-1}. Because the collection solid angle is small, there is no need to correct for the angular dependence of the differential Raman scattering cross section as was done in Ref. 8. At the wavelength that produces scattered photons at 844.5 nm, the value of $\langle d\sigma/d\Omega \rangle$ is equal to 3.56×10^{-31} cm^2/sr.

The Raman calibration was carried out by placing a small stainless steel cell, filled with hydrogen and equipped with Brewster-angle entrance and exit windows for the laser beam, inside the test cell. A Pyrex® view-port allowed scattered photons at right angles to the laser direction to escape. This window did not restrict the viewing region of the fluorescence collection lens. The path of the visible laser beam was the same as the path followed by the 226-nm beam, perpendicular to the flow direction. The polarization vector of the laser radiation was oriented parallel to the flow direction. The Scientech power meter was placed on the floor of the test cell to measure the laser pulse energy. The fluorescence collection system and detection electronics (including Ortec 113 preamp) were configured exactly as they had been in the O-atom number density measurement. The size of the aperture defining the observation region was checked by closing it down on a drill bit of known size (4.37 mm), as was done in the O-atom measurements. The signal amplitude and laser pulse energy were recorded as a function of laser wavelength. The Raman

Table 2 Values of the quantities used to calculate the atomic oxygen number density under the conditions of run 22, using Eq. (4)

Quantity	Value
S	0.032 V
E	7.0×10^{-4} J
ω_v	0.114 cm
ω_h	0.059 cm
$h\nu$	8.80×10^{-19} J
$\hat{\sigma}^{(2)}$	1.97×10^{-46} cm^4 s
ϕ_f	0.91
D	3.4×10^{-10} V cm sr
$\int F^2(t'')\, dt''$	1.7×10^8 s^{-1}
$N_0(J'' = 2)$ (experiment)	1.3×10^{15} cm^{-3}
$\Sigma N_0(J'' = 2, 1, 0)$ (experiment)	$(1.8 \pm 0.8) \times 10^{15}$ cm^{-3}
$\Sigma N_0(J'' = 2, 1, 0)$ (NOZNT)	1.0×10^{15} cm^{-3}

Table 3 Fine structure temperatures

Run	Geometric area ratio	T, K experiment	T, K NOZNT
16	256	461 ± 50	275
21	64	532 ± 50	560
22	64	514 ± 50	560

calibration constant was calculated at each wavelength using Eq. (8), after applying a small correction to account for reflection losses on the viewport.

The data used to calculate the atomic oxygen number density are shown in Table 2. The calculation takes place in two steps. First, the population in the $J'' = 2$ fine structure state is determined using Eq. (4). Then, using the measured relative populations in the three fine structure levels (discussed in the following subsection), the total population in the $2p^3P$ electronic state is calculated. For comparison, the calculated number density from the NOZNT code is also shown in Table 2.

Fine Structure Temperatures

The fine structure temperature should be very close to the local translational temperature. Ab initio calculations of rate constants for state-to-state fine structure collisional excitation and de-excitation by hydrogen predict numbers on the order of 10^{-10} cm^3 s^{-1} at 500 K.[23] The rate constants for larger collision partners should be at least as large as those for hydrogen. Using a typical number density of heavy particles in the flow (10^{16} cm^{-3}), a relaxation time of about 1 μs is estimated for equilibration among the fine structure levels. Because this time is much shorter than both the flow time between the nozzle exit and the point of observation (about 50 μs), and the transit time inside the nozzle (several hundred μs), equilibrium should be reached. Because heavy particles are the collisional partners in this relaxation process, the temperature characterizing the fine structure levels should equal the heavy particle translational temperature. This assumption is supported by experience with laboratory sources of oxygen atoms. In earlier experiments[9] using atoms created in a microwave discharge and then equilibrated with O_2 at room temperature in a flow system, the fine-structure relative populations (measured by two-photon LIF) approximated a room-temperature Boltzmann distribution.

Fine structure temperatures were determined as follows. During a single arcjet run lasting approximately 15 min, the laser was scanned through each of the three fine structure lines ($3p^3P_{2,1,0} \leftarrow 2p^3P_2$, $3p^3P_{2,1} \leftarrow 2p^3P_1$, and $3p^3P_{2,0} \leftarrow 2p^3P_0$). The laser beam path was kept constant as the wavelength was changed. The spatial and temporal profiles were certainly constant over the small range of wavelengths used. (The arc heater current, pressure, and voltage were held constant to within 2% throughout the run. In previous runs of the same

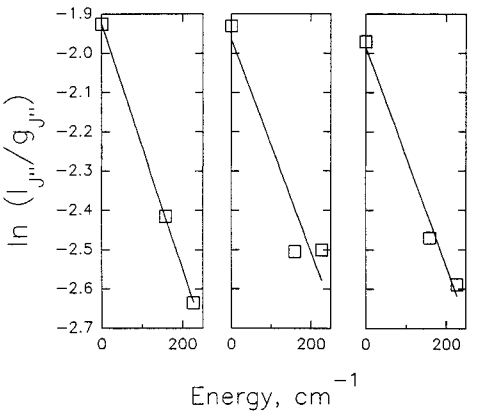

Fig. 5 Boltzmann plots for the fine structure levels of atomic oxygen (squares), along with least-squares fits to Boltzmann distributions (solid lines), runs 16, 20, and 22.

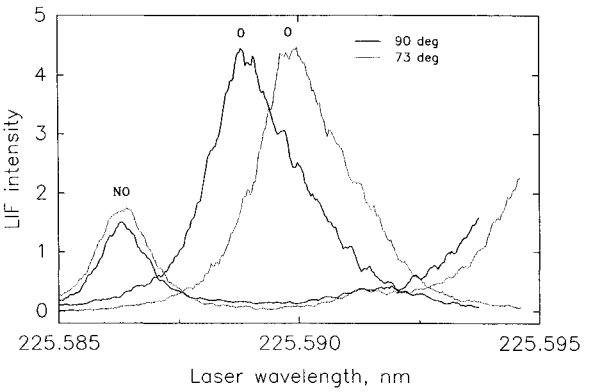

Fig. 6 LIF signals for nitric oxide (in a room temperature static gas cell) and atomic oxygen (in the arcjet) as a function of laser wavelength.

length under similar conditions, the observed LIF signal on a single transition showed no detectable systematic change during the run.) For each of the three lines the signal, properly normalized for pulse energy fluctuations, was measured as a function of wavelength. Examples of such spectra were shown earlier in Fig. 3. The integrated areas of these curves, which are proportional to the population in the fine structure state forming the lower level of the transition, were recorded. The natural logarithm of $(I_{J''}/g_{J''})$ was plotted as a function of the energy $E_{J''}$ to produce "Boltzmann plots" (shown in Fig. 5) from which the temperature could be calculated. The least-squares fits to straight lines yield the fine structure temperatures shown and compared with theory in Table 3.

Atomic Oxygen Velocity Measurements

The physical basis of the velocity measurements is as follows. If an ensemble of atoms has a nonzero average velocity component along the direction of laser propagation, the position of the absorption resonance will be shifted relative to the resonance position in the case of stationary atoms. The velocity is calculated from the magnitude of this shift.

In preliminary experiments atomic copper sputtered from electrodes was used as the target species, but the results were unacceptable because the local atomic density fluctuated wildly during the course of a given run and declined steadily from run to run as the electrodes aged. In subsequent experiments atomic oxygen, a major component of the flow that provided much more reliable results, was used as the target species.

The procedure for measuring velocities consisted of three steps:

1) Measure the splitting between the O-atom line and the nearest nitric oxide line at $\theta = 90$ deg.

2) Measure the splitting between the O-atom line and the same nitric oxide line at fixed value of θ less than 90 deg.

3) Calculate the flow velocity from the following equation:

$$v = \frac{c(\Delta\lambda_\theta - \Delta\lambda_{90})}{\lambda \cos\theta} \tag{10}$$

Examples of the data used in the velocity measurements are shown in Fig. 6. The dotted lines show spectra at $\theta = 73$ deg, run 5, while the solid lines show spectra at $\theta = 90$ deg, run 12. In both cases the spectrum with a peak at ~225.586 nm is the NO reference spectrum. This peak is the $R_1(16)$ transition in the $\gamma(0,0)$ band of $^{15}N^{16}O$, an isotopic species with a 0.3% abundance in the sample of natural nitric oxide.

Values of $(\Delta\lambda_\theta - \Delta\lambda_{90})$ were derived from the spectra using the least-squares curve fitting. To describe the asymmetric shape of the $3p^3P_{2,1,0} \leftarrow 2p^3P_2$ transition (which consists of three overlapped lines), the positions and relative intensities of the three lines, which are known from Doppler-free spectroscopy,[10] were used. The fitted position of the strongest component, the $3p^3P_2 \leftarrow 2p^3P_2$ line, was defined as the O-atom peak position and its spacing relative to the fitted position of the $R_1(16)$ line of $^{15}N^{16}O$ was measured. The best fits were obtained using Lorentzian fits to the O-atom peaks and Gaussian fits to the NO peaks. The results, along with calculations from the ACE and NOZNT codes, are presented in Table 4 and shown graphically in Fig. 7. In that figure, the abscissa is the mass-averaged enthalpy calculated by the ARCFLO code.

The data from runs 7 and 8 provide some information about the radial dependence of the velocity. The quantity r is the distance of the observation point above the centerline of the flow. Although the $r = 0$ cm and $r = 15$ cm data were taken during two different arcjet runs, the conditions were nearly identical. Because the average observed velocity at $r = 15$ cm (4.40 ± 0.10 km/s) matches the velocity at $r = 0$ cm (4.41 km/s), the velocity seems independent of radial position over at least a 15-cm range for expansion through a 61-cm nozzle. (The off-axis velocity was corrected for imperfect collimation by assuming that the atoms move in a straight line from the throat to the point of observation).

Table 4 Summary of O-atom velocity measurements

Run	r, cm	v, obs	v, ACE	v, NOZNT
4	0	4.93 ± 0.3	4.53	5.49
4	0	4.98 ± 0.3	——	——
5	0	4.51 ± 0.3	4.43	——
6	0	5.67 ± 0.3	4.08	5.69
7	0	4.41 ± 0.3	4.04	5.05
7	0	4.41 ± 0.3	——	——
8	15	4.37 ± 0.3	4.07	5.02
8	15	4.52 ± 0.3	——	——
8	15	4.32 ± 0.3	——	——

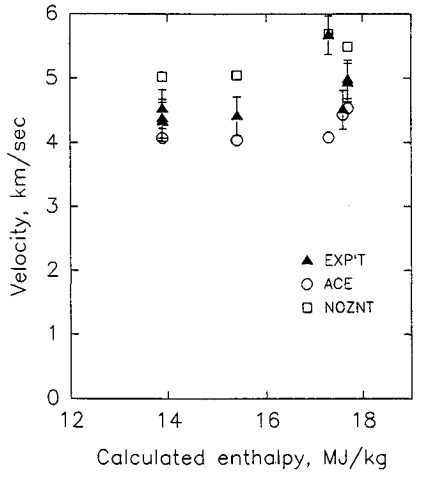

Fig. 7 Comparison of observed and calculated O-atom velocities.

Error Estimates

The biggest source of error in the number density measurement is uncertainty about the value of $\hat{\sigma}^{(2)}$, because of the unknown photon statistical factor $G^{(2)}$. The true value of $\hat{\sigma}^{(2)}$ could differ by ±36% (±0.8/2.2) from the assumed value. Five of the six other experimentally determined quantities in Eq. (4) [ω_v, ω_h, ϕ_f, D, and $\int F^2(t'')\,dt''$] have each been measured to a precision of 5–10%, whereas the sixth quantity, S/E^2, has been measured to a precision of 3%. Adding these errors in quadrature, a total error of about 25% for the quantity $[N_0\hat{\sigma}^{(2)}]$ is obtained. (This error limit is consistent with earlier work[10] in which the two-photon cross section was measured to a precision of ±30%.) Adding this error in quadrature with the 36% error in $\hat{\sigma}^{(2)}$, a total error limit of ±44% is obtained for N_0. In the velocity measurements the combined random error (from the noise in the spectra) and systematic error (from imperfect measurement of θ, ±0.5 deg) is approximately 0.3 km/s. In the fine structure temperature measurement the individual relative peak intensities are reproducible to within 3%, corresponding to an uncertainty of ±50 K in the fine structure temperature.

Discussion

Two major components of the arcjet flow, $O(2p^3P)$ and $N(2p^4S^0)$, have been detected by laser-induced fluorescence. To our knowledge, this represents the first direct detection of either species in the freestream of an arcjet flow.

The observed and calculated O-atom densities agree moderately well with the experimental number density being slightly higher than the calculated density. Three facts should be noted in interpreting this result. First, the NOZNT code calculates virtually complete dissociation of O_2 under the entire range of enthalpies produced by the arc heater. The uncertainty about the true value of the enthalpy is too small to take the flow out of the fully dissociated regime for O_2 under the conditions of the number density measurement. Thus, the impact pressure is proportional to the product N_0v^2. Second, the composition of the test gas (80% air, 20% argon) is well-known from experimental flow rate measurements. Third, the observed impact pressure is accurately reproduced in the NOZNT calculations. If the calculated value of N_0 is too low, then the calculated velocity must be too high, in qualitative agreement with the trend shown in Fig. 7. The accuracy of the number density measurement can be improved by calibrating the measurement against a laboratory O-atom source with a known density. The same procedure can be used to measure the N-atom number density, which is very sensitive to the centerline enthalpy. Measurements of atomic oxygen number density, atomic nitrogen number density, and flow velocity under a single set of test conditions are needed to resolve the small discrepancy raised by this first number density measurement.

In two of the three cases shown in Table 3, the observed fine structure temperature is in reasonably good agreement with the translational temperatures calculated using NOZNT. This result is consistent with earlier measurements of NO rotational temperatures[15] that also agreed with the predictions of NOZNT. In one case, the measured fine structure temperature is much higher than the calculated translational temperature. The reason for this discrepancy is not known. Since the NOZNT calculations rely on assumptions about collisional relaxation rates that may not be accurate, and since the equality between heavy particle transitional temperature and fine structure temperature may not hold at low densities, this lack of agreement is not completely surprising. Further experiments covering a variety of operating conditions should clarify this issue.

The observed velocities are systematically higher than the velocities calculated using the ACE code, which is to be expected for two reasons: 1) the assumed enthalpy is too low to be consistent with the existing body of experimental data,[15]

and 2) the assumption of frozen chemistry precludes N-atom recombination in the nozzle. As noted above, the NOZNT code predicts velocities that are systematically higher than the observed velocities by about 10%. The reason for this discrepancy is not clear. The calculations can be improved through a better knowledge of N-atom recombination rates and nonthermal electronic population distributions, whereas the experimental uncertainty can be reduced by exciting the flow at a smaller incidence angle and using a laboratory O-atom source as a zero-velocity reference.

Although flow velocities and translational temperatures have been measured at NASA Johnson Space Center using atomic copper as a probe,[4,5] these results cannot yet be compared with the present results because the flow conditions and computer codes used to predict the flow properties are different in the two cases.

Summary and Conclusions

A laser-induced fluorescence sensor has provided new information about the properties of the arcjet flow at the NASA Ames Aerodynamic Heating Facility. The number density of $O(2p^3P)$ is $(1.8 \pm 0.8) \times 10^{15}$ cm^{-3} for one set of conditions, in fair agreement with predictions from the NOZNT code. The fluorescence quenching rates for $O(3p^3P)$ and $N(3p^4D^0)$ are surprisingly small under all conditions, and they are consistent with quenching by heavy particles alone. The three fine structure levels of $O(2p^3P)$ are in thermal equilibrium at temperatures near 500 K, which should approximate the local translational temperature. Good agreement between measured fine structure temperatures and calculated translational temperatures (from NOZNT) was obtained in two out of three cases. The velocities of atomic oxygen under most conditions are between 4–5 km/s. They are slightly larger than predicted from the ACE computer code that assumes frozen chemistry, and are in moderately good agreement with the NOZNT code that includes detailed chemical rate calculations.

Acknowledgment

The experimental work was funded through the NASA Small Business Innovation Research Program under Contract NAS2-13469.

References

[1]Park, C., *Nonequilibrium Hypersonic Aerothermodynamics*, Wiley, New York, 1990.

[2]Sharma, S. P., and Park, C., "Survey of Simulation and Diagnostic Techniques for Hypersonic Nonequilibrium Flows," *Journal of Thermophysics and Heat Transfer*, Vol. 4, No. 2, 1990, pp. 129–142.

[3]Scott, C. D., "Survey of Measurements of Flow Properties in Arcjets," *Journal of Thermophysics and Heat Transfer*, Vol. 7, No. 1, 1993, pp. 9–24.

[4]Arepalli, S., Yuen, E. H., and Scott, C. D., "Application of Laser Induced Fluorescence for Flow Diagnostics in Arc Jets," AIAA Paper 90-1763, June 1990.

[5]Marinelli, W. J., Kessler, W. J., Allen, M. G., and Davis, S. J., "Copper Atom Based Measurements of Velocity and Turbulence in Arc Jet Flows," AIAA Paper 91-0358, Jan. 1991.

[6]Gopaul, N. K. J. M., "Spectral Measurement of Nonequilibrium Nitric Oxide in the Free-Stream of an Arc-Jet Flow," M.S. Thesis, Stanford Univ., Stanford, CA, Aug. 1992.

[7]Engleman, R., Jr., Rouse, P. E., Peek, H. M., and Baiamonte, V. D., "Beta and Gamma Band Systems of Nitric Oxide," Los Alamos Scientific Lab. Rept. LA-4364, Los Alamos, NM, Oct. 1969.

[8]Bischel, W. K., Bamford, D. J., and Jusinski, L. E., "Absolute Calibration of a Fluorescence Collection System by Raman Scattering in H_2," *Applied Optics*, Vol. 25, No. 7, 1986, pp. 1215–1221.

[9]Bamford, D. J., Jusinski, L. E., and Bischel, W. K., "Absolute Two-Photon and Three-Photon Ionization Cross Sections for Atomic Oxygen," *Physical Review A*, Vol. 34, No. 1, 1986, pp. 185–198.

[10]Bamford, D. J., Dyer, M. J., and Bischel, W. K., "Single-Frequency Laser Measurements of Two-Photon Cross Sections and Doppler-Free Spectra for Atomic Oxygen," *Physical Review A*, Vol. 36, No. 7, 1987, pp. 3497–3500.

[11]Bamford, D. J., Hickman, A. P., Dyer, M. J., and Bischel, W. K., "Comparative Photon Statistics of Several Ultraviolet Laser Systems Determined by Transient Two-Photon Absorption," *Journal of the Optical Society of America B*, Vol. 5, No. 7, 1988, pp. 1369–1378.

[12]Yoshikawa, K. K., and Katzen, E. D., "Charts for Air-Flow Properties in Equilibrium and Frozen Flows in Hypervelocity Nozzles," NASA TN D-693, April 1961.

[13]Gupta, R. N., Yos, J. M., Thompson, R. A., and Lee, K.-P., "A Review of Reaction Rates and Thermodynamic and Transport Properties for an 11-Species Air Model for Chemical and Thermal Nonequilibrium Calculations to 30000 K," NASA RP 1232, Aug. 1990.

[14]Anon., "Aerotherm Chemical Equilibrium Program (ACE81)," Accurex Corp., Rept. UM81-11/ATD, Mountain View, CA, Aug. 1981.

[15]Babikian, D. S., Gopaul, N. K. J. M., and Park, C., "Measurement and Analysis of Nitric Oxide Radiation in an Arc-Jet Flow," AIAA Paper 93-2800, July 1993.

[16]Saxon, R. P., and Eichler, J., "Theoretical Calculation of Two-Photon Absorption Cross Sections in Atomic Oxygen," *Physical Review A*, Vol. 34, No. 1, 1986, pp. 199–206.

[17]Wiese, W. L., Smith, M. W., and Glennon, B. M., *Atomic Transition Probabilities*, U.S. Government Printing Office, Washington, DC, 1966.

[18]Copeland, R. A., Jeffries, J. B., Hickman, A. P., and Crosley, D. R., "Radiative Lifetime and Quenching of the $3p^4D^0$ State of Atomic Nitrogen," *Journal of Chemical Physics*, Vol. 86, No. 9, 1987, pp. 4876–4884.

[19]Meier, U., Kohse-Hoinghaus, K., and Just, T., "H and O Atom Detection for Combustion Applications: Study of Quenching and Laser Photolysis Effects," *Chemical Physics Letters*, Vol. 126, No. 6, 1986, pp. 567–573.

[20]Huang, Y.-L., and Gordon, R. J., "The Effect of Amplified Spontaneous Emission on the Measurement of the Multiplet State Distribution of Ground State Oxygen Atoms," *Journal of Chemical Physics*, Vol. 97, No. 9, 1992, pp. 6363–6368.

[21]Hancock, G., and Toogood, M. J., "Laser-Induced Fluorescence of Oxygen Atoms in a Plasma Reactor," *Applied Physics Letters*, Vol. 60, No. 1, 1992, pp. 35–37.

[22]Alden, M., Westblom, U., and Goldsmith, J. E. M., "Two-Photon Excited Stimulated Emission from Atomic Oxygen in Flames and Cold Gases," *Optics Letters*, Vol. 14, No. 6, 1989, pp. 305–307.

[23]Jaquet, R., Staemmler, V., Smith, M. D., and Flower, D. R., "Excitation of the Fine-Structure Transitions of $O(^3P_J)$ in Collisions with Ortho- and Para-H_2," *Journal of Physics B: Atomic, Molecular, and Optical Physics*, Vol. 25, No. 1, 1992, pp. 285–297.